Neurobiology of Disease 62 (2014) 407–415

Contents lists available at ScienceDirect

Neurobiology of Disease

journal homepage: www.elsevier.com/locate/ynbdi

Endogenous murine tau promotes neurofibrillary tangles in 3xTg-AD mice without affecting cognition

David Baglietto-Vargas [a], Masashi Kitazawa [a,b], Elaine J. Le [a], Tatiana Estrada-Hernandez [a], Carlos J. Rodriguez-Ortiz [a,b], Rodrigo Medeiros [a], Kim N. Green [a], Frank M. LaFerla [a,*]

[a] Department of Neurobiology and Behavior, Institute for Memory Impairments and Neurological Disorders, University of California, Irvine, CA 92697-4545, USA
[b] Department of Molecular and Cell Biology, University of California, Merced, CA 95343, USA

ARTICLE INFO

Article history:
Received 21 March 2013
Revised 1 October 2013
Accepted 22 October 2013
Available online 29 October 2013

Keywords:
Alzheimer's disease
Tau
Hippocampus
3xTg-AD mice
Neurofibrillary tangles

ABSTRACT

Recent studies on tauopathy animal models suggest that the concomitant expression of the endogenous murine tau delays the pathological accumulation of human tau, and interferes with the disease progression. To elucidate the role of endogenous murine tau in a model with both plaques and tangles, we developed a novel transgenic mouse model by crossing 3xTg-AD with mtauKO mice (referred to as 3xTg-AD/mtauKO mice). Therefore, this new model allows us to determine the pathological consequences of the murine tau. Here, we show that 3xTg-AD/mtauKO mice have lower tau loads in both soluble and insoluble fractions, and lower tau hyperphosphorylation level in the soluble fraction relative to 3xTg-AD mice. In the 3xTg-AD model endogenous mouse tau is hyperphosphorylated and significantly co-aggregates with human tau. Despite the deletion of the endogenous tau gene in 3xTg-AD/mtauKO mice, cognitive dysfunction was equivalent to 3xTg-AD mice, as there was no additional impairment on a spatial memory task, and thus despite increased tau phosphorylation, accumulation and NFTs in 3xTg-AD mice no further effects on cognition are seen. These findings provide better understanding about the role of endogenous tau to Alzheimer's disease (AD) pathology and for developing new AD models.

Introduction

Alzheimer's disease (AD) is a progressive neurological disorder associated with senile dementia among elderly populations. The afflicted brain contains several pathological hallmarks, including extracellular Aβ-amyloid plaques, intraneuronal neurofibrillary tau tangles (NFTs) and extensive neuronal and synaptic loss (Querfurth and LaFerla, 2010). It is believed that these hallmark pathologies are related, with overwhelming evidence showing that pathological conformations of Aβ can trigger the abnormal hyperphosphorylation of tau and lead to NFTs (Gotz et al., 2001; Lewis et al., 2001; Oddo et al., 2004, 2008; Tseng et al., 2008). Additionally, recent animal studies have shown that tau protein is necessary for Aβ to cause memory impairments, thus cementing the detrimental relationship between the two pathological proteins (Brion et al., 1999; Medeiros et al., 2011; Roberson et al., 2007; Shipton et al., 2011). Hence, these studies suggest that tau is an important enactor of Aβ-induced cognitive decline and neurodegeneration.

Tau is a neuron-specific cytoskeletal protein that is directly involved in maintaining the integrity, stability and dynamics of microtubules (Medeiros et al., 2011; Terwel et al., 2002). Moreover, there is recent evidence suggesting that tau exerts an important role in signal transduction, neurite outgrowth and stabilization during brain development and interaction with actin cytoskeleton (Denk and Wade-Martins, 2009; Hernandez and Avila, 2007). Tau exists as an unfolded form and mainly associated to microtubules (MT) in the brain; however, in several neurodegenerative disorders, tau is highly phosphorylated and becomes characteristically insoluble. This insolubility leads to aggregation of NFT in selected brain regions. These pathological changes are observed in AD and other human tauopathies such as Pick's disease (PiD), progressive supranuclear palsy (PSP), corticobasal degeneration (CBD), argyrophilic grain disease and frontotemporal dementia with parkinsonism linked to chromosome 17 (FTDP-17) (Denk and Wade-Martins, 2009; Hernandez and Avila, 2007).

Several transgenic lines have been created that model human tauopathies, via overexpression of FTD-associated mutant tau transgenes in neurons (Medeiros et al., 2011). These models show increased hyperphosphorylated tau, most of them eventually form NFTs, and show neurodegeneration. It is important to note that these transgenic lines contain endogenous murine tau, in addition to the mutant human tau produced by the transgenes. Several studies have shown that the presence of this endogenous murine tau delays the pathological accumulation of human tau (Brion et al., 1999; Duff et al., 2000; Gotz et al., 1995; Higuchi et al., 2002; Ishihara et al., 1999, 2001; Probst et al., 2000). In other words, when the endogenous murine tau is removed from transgenic tau mice, the onset and the progression of AD-like NFT and paired helical filament (PHF) aggregates are accelerated (Ando et al., 2011;

* Corresponding author at: Department of Neurobiology and Behavior, Institute for Memory Impairments and Neurological Disorders (UCI MIND), 3212 Biological Sciences III, Irvine, CA 92697-4545, USA. Fax: +1 949 824 7356.
E-mail address: laferla@uci.edu (F.M. LaFerla).
Available online on ScienceDirect (www.sciencedirect.com).

0969-9961/$ – see front matter © 2013 Published by Elsevier Inc.
http://dx.doi.org/10.1016/j.nbd.2013.10.019

Andorfer et al., 2003). These studies suggest that the endogenous murine tau interferes with human tau aggregation and toxicity by unknown mechanisms.

To model human AD, we created the 3xTg-AD mice in which both human mutant APP and tau were overexpressed in neurons. These mice develop both plaques and tangles, and have been used to show the relationship between the development of Aβ and tau pathologies (Billings et al., 2005; Oddo et al., 2003, 2004, 2007, 2008; Tseng et al., 2008). We have now generated a 3xTg-AD mouse model in the absence of the endogenous murine tau. This novel transgenic line, referred to as 3xTg-AD/mtauKO, is devoid of any murine tau protein, the only tau present is human and expressed only in cells with the human transgene — namely neurons in the hippocampus, cortex and amygdala. We hypothesize that 3xTg-AD/mtauKO mice exhibit more accurate molecular interactions between human Aβ and tau without the endogenous murine tau interference. Interestingly, we find that the 3xTg-AD mice have increased levels of hyperphosphorylated tau and, NFTs versus 3xTg-AD/mtauKO mice. Moreover, the increases in tau hyperphosphorylation and NFT formation observed in the 3xTg-AD are not associated with additional impairment on a spatial memory task when compared with 3xTg-AD/mtauKO mice. Hence, our study suggests that the endogenous murine tau contributes to the pathologies seen in 3xTg-AD mice by increasing phosphorylated forms of tau and NFTs. However, these increases in tau pathology (NFTs) are not correlated with further cognitive impairment.

Material and methods

Transgenic mice

The characterization of 3xTg-AD mice has been described previously (Oddo et al., 2003). Briefly, two independent transgenes encoding human APP_{Swe} and the human tau_{P301L} (both under control of the mouse Thy1.2 regulatory element) were co-microinjected into single-cell embryos harvested from homozygous mutant $PS1_{M146V}$ knockin (PS1-KI) mice (Oddo et al., 2003). We crossed the 3xTg-AD mice with tau knockout mice generated in the laboratory of Dr. Vitek (Dawson et al., 2001). Through careful breeding, we derived a colony of 3xTg-AD mice that lack both copies of the endogenous mouse wild type tau gene (i.e., $hPS1KI_{M146V}$/$hPS1KI_{M146V}$; $hAPP_{SWE}$/$hAPP_{SWE}$; $hTau_{P301L}$/$hTau_{P301L}$; mTau −/−; where h = human and m = mouse gene). We refer these mice as the 3xTg-AD/mtauKO. In this work, 18 months of age homozygous Non-transgenic (Ntg), tau knockout (mtauKO), 3xTg-AD and 3xTg-AD/mtauKO, 16–20 per group (males and females) was used. Both 3xTg-AD and 3xTg-AD/mtauKO mice were homozygous for APP and tau transgenes. Mice (Ntg, mtauKO, 3xTg-AD and 3xTg-AD/mtauKO) have the same genetic background (hybrid 129/C57BL6 background). All animal procedures were performed in accordance with the National Institutes of Health and University of California guidelines and Use Committee at the University of California, Irvine.

Behavioral test

Novel context and place recognition

Before testing, each mouse was habituated to an empty Plexiglas arena (45 × 25 × 20 cm) for 3 consecutive days. The lighting intensity in each behavioral task was measured at 44 lx. The arena and the objects were cleaned thoroughly between trials to ensure the absence of olfactory cues. If an animal did not explore both objects during the training phase, the test was not scored. Because some mice exhibited freezing behavior when placed in the arena, test did not start until the mouse moved from its starting position, which was always in the corner closest to the familiar object. Exploration was considered when the mouse's head was within 2.5 cm of the object, with its neck extended and vibrissae moving. Simple proximity, chewing, or standing on the object did not count as exploratory behavior. All exploratory segments and tests were videotaped for scoring purposes.

For novel context, mice were exposed to two identical objects (i.e., balls) in a round Plexiglas arena for 5 min and 30 min later two other identical objects (i.e., small cubes) in a rectangular cage for 5 min. After 24 h, mice were placed into either the round or the rectangular Plexiglas arena in which one of the objects was novel for that context (i.e., a ball and small cube are placed into the round Plexiglas arena). The recognition index represents the percentage of the time that mice spend exploring the novel object (Baglietto-Vargas et al., 2013).

Morris water maze

Morris water maze tests were conducted as described previously (Baglietto-Vargas et al., 2013; Billings et al., 2005; Medeiros et al., 2011). Mice were trained to swim to a 14 cm diameter circular Plexiglas platform submerged 1.5 cm beneath the surface of the water and invisible to the mice while swimming. The platform was located in a fixed position, equidistant from the center and the wall of the tank. Mice did four training trials per day. During each trial, mice were placed into the tank at one of four designated start points in a pseudorandom order. Mice were trained for as many days as needed to reach the training criterion of 25 s (escape latency). If the mice failed to find the platform within 60 s, they were manually guided to the platform and allowed to remain there for 5 s. The probe was assessed 24 h after the last training session and consisted of a 60-s trial without the platform. Performance was monitored with the EthoVision XT video tracking system.

Tissue preparation

After deep anesthesia with sodium pentobarbital (60 mg/kg), Ntg, mtauKO, 3xTg-AD and 3xTg-AD/mtauKO mice were perfused transcardially with 0.1 M phosphate-buffered saline (PBS), pH 7.4. Half of the brain was fixed for 48 h in 4% paraformaldehyde in 0.1 M phosphate buffer saline, pH 7.4 and cryoprotected in 30% sucrose for immunohistochemical analysis, whereas the other half was frozen in dry ice for biochemical analysis. Thick (40 μm) free-floating sections were obtained using a freezing microtome (Leica SM 2010 R) and serially collected (each series contained sections that represented 1/7th of the total brain) in cold PBS and 0.02% sodium azide.

Protein extracts were prepared by homogenizing whole brain hemisphere samples in T-per (Thermo Fisher Scientific, Rockford, IL) extraction buffer (150 mg/ml), complemented with a protease inhibitor (Complete Mini Protease Inhibitor Tablets, Roche Diagnostics GmbH, Germany) and phosphatase inhibitor (5 mmol/l, Sigma-Aldrich, St. Louis, MO), followed by centrifugation at 100,000 ×*g* for 1 h. Protein concentration in the supernatant was determined using the Bradford assay.

For insoluble protein extraction and analysis, Acetone/TCA precipitation protocol was used (Fic et al., 2010). Briefly, insoluble proteins were homogenizing with 70% formic acid (Thermo Fisher Scientific, Rockford, IL), followed by centrifugation at 100,000 ×*g* for 1 h. Supernatant was collected and the formic acid of the supernatant was neutralized using the following ration (1 volumen of sample, 1 volumen of neutralization buffer and 1.8 volumenes 10 N of NaOH). Then, each volumen of sample was mixed with 10 volumenes of cold 10% TCA (Trichloroacetic acid; Thermo Fisher Scientific) in Acetone (Thermo Fisher Scientific) at −20 °C overnight. Next, samples were centrifugated at 15,000 ×*g* for 10 min and the supernatant was removed. Then, cold acetone was added and incubated at −20 °C for 10 min. After that, samples were centrifugated at 15,000 ×*g* for 15 min. Supernatant was removed and the pellet was air-dried. The pellet was re-solubilized in T-per (Thermo Fisher Scientific) extraction buffer (150 mg/ml), complemented with a protease inhibitor (Complete Mini Protease Inhibitor

Tablets, Roche Diagnostics GmbH) and phosphatase inhibitor (5 mmol/l, Sigma-Aldrich).

Immunohistochemistry

Coronal free-floating sections (40 μm thick) were pretreated with 3% H_2O_2/3% methanol in Tris-buffered saline (TBS) for 30 min to block endogenous peroxide activity. After TBS wash, sections were incubated first in TBS with 0.1% Triton X-100 (TBST) for 15 min, and then in TBST with 2% bovine serum albumin (BSA, Sigma-Aldrich) for 30 min. Sections were incubated with anti-6E10 (Covance Research Products, Denver, PA, USA) in TBS + 5% normal goat or horse serum overnight at 4 °C. Sections were then incubated with biotinylated anti-mouse; 1:500 in TBS + 2% BSA + 5% normal serum for 1 h at 20 °C, followed by Vector ABC Kit and DAB reagents (Vector Laboratories, Burlingame, CA, USA) to visualize staining. Sections were mounted on gelatin-coated slides, dehydrated in graded ethanol, cleared with xylene and coverslipped with DPX (BDH) mounting medium. The specificity of the immune reactions was controlled by omitting the primary antibody.

Immunofluorescence

Coronal free-floating sections (40 μm thick) were pretreated with 3% H_2O_2/3% methanol in Tris-buffered saline (TBS) for 30 min to block endogenous peroxide activity. After TBS wash, sections were incubated once in TBS with 0.1% Triton X-100 (TBST) for 15 min, and once in TBST with 2% bovine serum albumin (BSA, Sigma-Aldrich) for 30 min. Sections were incubated with anti-MAP2 (1:1000, Abcam, Cambridge, MA); anti-PHF1 (Dr. Peter Davies, Albert Einstein College of Medicine, Manhasset, NY, USA) in TBS + 5% normal goat or horse serum overnight at 4 °C. Sections were then rinsed and incubated for 1 h with secondary Alexa Fluor-conjugated antibody (Invitrogen, Carlsbad, CA, USA) at room temperature. Finally, sections were mounted onto gelatin-coated slides in Fluoromount-G (Southern Biotech, Birmingham, AL, USA) and examined under a Leica DM2500 confocal laser microscope.

The immunostaining was assessed at five brain coronal levels, between −1.46 anterior and −3.08 mm posterior to Bregma, according to the atlas of Paxinos and Watson (n = 8 animals per group). Specifically, we captured 1–2 images per section with 10× objective in the subiculum and CA1 hippocampal subfield using a Leica DM2500 confocal laser microscope. A threshold optical density that best discriminated the staining from the background was obtained using ImageJ 1.36b imaging software. The data represents the average value obtained by the analysis of images of the hippocampus (subiculum and CA1). All histological assessments were performed by an examiner blinded to sample identities.

Gallyas silver staining

Conventional Gallyas silver staining was performed to identify hyperphosphorylated tau fibrils and aggregates (Braak et al., 1988; Gallyas, 1971). Gallyas silver staining was assessed at four brain coronal levels, between −1.46 anterior and −3.08 mm posterior to Bregma, according to the atlas of Paxinos and Watson (n = 8 animals per group). Specifically, we captured the hippocampal images with 10× objective using a Carl Zeiss microscope. A threshold optical density that best discriminated the staining from the background was obtained using ImageJ 1.36b imaging software. The data represents the average value obtained by the analysis of images of the hippocampus. All histological assessments were performed by an examiner blinded to sample identities.

Immunoblotting

Equal amounts of protein (20 μg) were separated on 4–12% Bis-Tris gel (Invitrogen, Carlsbad, CA), transferred to the nitrocellulose membranes. Membranes were blocked for 1 h in 5% (w/v) suspension of nonfat milk in 0.2% Tween 20 Tris-buffered saline (pH 7.5). After blocking, the membranes were incubated overnight at 4 °C, with one of the following primary antibodies: anti-6E10 (1:1000, Covance Research Products), anti-Cdk5 (1:1000) and CTF20 (1:5000) for C99 and C83 (Calbiochem, San Diego, CA, USA), HT7 (1:5000), AT8 (1:1000), AT100 (1:1000), AT180 (1:1000) and AT270 (1:1000) (Thermo Scientific), PHF1 (Dr. Peter Davies, Albert Einstein College of Medicine, Manhasset, NY, USA), poly-tau (1:3000; Dako, Carpinteria, CA, USA), anti-pGSK3β (ser9) (1:1000) (Cell Signaling Technology, Danvers, MA, USA), anti-C-term p35 (1:200) for p25 and p35, and GAPDH (1:5000, Santa Cruz Biotechnology, Santa Cruz, CA, USA). The membranes were washed in Tween–TBS for 20 min and incubated at 20 °C with the specific secondary antibody at a dilution of 1:10,000 (Pierce Biotechnology) for 60 min. The blots were developed using Super Signal (Thermo Scientific).

Enzyme-linked immunosorbent assay for $A\beta_{40}$ and $A\beta_{42}$

$A\beta_{1-40}$ and $A\beta_{1-42}$ were measured using a sensitive sandwich ELISA system as previously described (Baglietto-Vargas et al., 2013).

Quantitative and statistical analyses

All immunoblot data were quantitatively analyzed using Image J 1.36b software. The data were subsequently analyzed by Student's *t*-test comparison or one-way analysis of variance (ANOVA) using the Graphpad Prism software (Graphpad Prism Inc., San Diego, CA, USA). The significance was set at 95% of confidence. All values are presented as mean ± SEM.

Results

Endogenous murine tau deletion in 3xTg-AD/mtauKO mice

To study the pathological involvements of the endogenous murine tau in a transgenic mouse model of AD with plaques and tangles, we crossed the 3xTg-AD mice with mtauKO mice. The resulting transgenic mice (3xTg-AD/mtauKO) harbored APPswe (+/+), $PS1_{M146V}$ (+/+), tau_{P301L} (+/+) and no expression of murine endogenous tau (−/−), enabling us to examine the pathological interactions and involvements of the murine endogenous tau by directly comparing with 3xTg-AD mice. Western-blot analyses showed complete absence of steady-state levels of endogenous tau in mtauKO compared to Ntg mice (95.40 ± 0.79% one way ANOVA, Bonferroni post-hoc ***$p < 0.001$) (Fig. 1). Furthermore, we found reductions of tau steady-state levels in 3xTg-AD/mtauKO mice compared to 3xTg-AD mice (73.35 ± 2.26% one way ANOVA, Bonferroni post-hoc ***$p < 0.001$) (Fig. 1). These results are consistent with deletion of endogenous murine tau in 3xTg-AD/mtauKO animals. Notably, 3xTg-AD mice showed significantly higher levels of total tau compared to Ntg, due to the presence of both, endogenous and human transgenic tau (30.08 ± 0.91% one way ANOVA, Bonferroni post-hoc *$p < 0.05$) (Fig. 1). Additionally, we observed multiple tau bands at low molecular weights that could be generated by tau cleavage, and/or possible tau degradation.

3xTg-AD/mtauKO mice express lower levels of soluble and insoluble tau compared to 3xTg-AD mice

We next analyzed the soluble and insoluble tau protein levels in the 3xTg-AD/mtauKO and 3xTg-AD mice. Steady-state levels of total soluble tau are reduced in 3xTg-AD/mtauKO mice compared to 3xTg-AD mice, as are several tau fragments (Figs. 2A and B). Interestingly, significant reductions of total tau levels (68.50 ± 3.81%, ***$p < 0.001$, *t*-test) and tau positive bands were detected at 80 kDa (94.40 ± 2.49%, ***$p < 0.001$, *t*-test) and 28 kDa (97.95 ± 0.94%, ***$p < 0.001$, *t*-test)

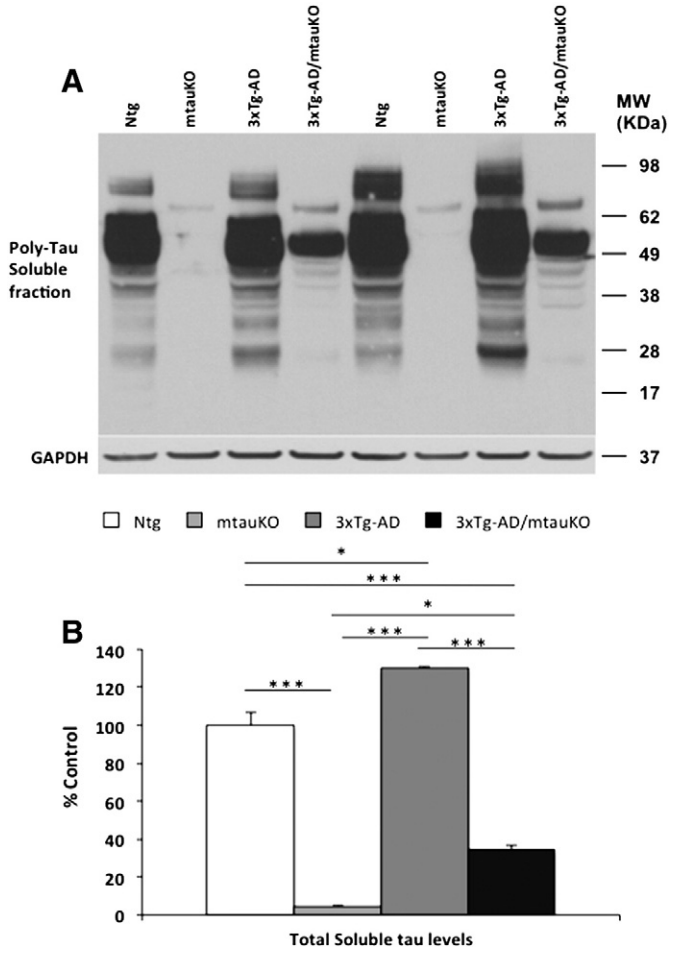

Fig. 1. Tau protein levels. A) Immunoblot analysis of total tau expression (poly-tau) from soluble (A) whole-brain homogenates in Ntg, mtauKO, 3xTg-AD and 3xTg-AD/mtauKO mice at 18 month-old (n = 4) shown as alternating lanes. B) Quantification of A normalized to GAPDH and expressed as a % of control shows significant decreases on total tau at 18 month-old in mtauKO compared to Ntg mice (95.40 ± 0.79% one way ANOVA, Bonferroni post-hoc ***p < 0.001) and in 3xTg-AD/mtauKO compared to 3xTg-AD mice (73.35 ± 2.26% one way ANOVA, Bonferroni post-hoc ***p < 0.001). In addition, significant increases in tau levels are observed in 3xTg-AD versus Ntg mice (30.08 ± 0.91% one way ANOVA, Bonferroni post-hoc *p < 0.05). GAPDH levels were used as control for protein loading. The values represent the mean ± S.E.M. *p < 0.05 and ***p < 0.001. Note: The measure of total tau expression was performed using all tau immunoreactive bands in each animal.

in 3xTg-AD/mtauKO versus 3xTg-AD mice (Fig. 2B). Additionally, we examined the detergent insoluble brain homogenate fraction, and found significant increases in total insoluble tau levels (89.32 ± 2.40%, **p < 0.01, *t*-test) and insoluble tau fragments at 52 kDa (66.93 ± 9.35%, **p < 0.01, *t*-test) and 28 kDa (97.11 ± 0.49%, **p < 0.01, *t*-test) in 3xTg-AD compared to 3xTg-AD/mtauKO mice (Figs. 2C and D). Gallyas silver staining further confirmed an increase (86.33 ± 28.17%, **p < 0.01, *t*-test) in the number of intraneuronal NFTs in the pyramidal cell layer of the hippocampus in the 3xTg-AD compared to the 3xTg-AD/mtauKO mice (Fig. 2E). In addition, a significant number of dystrophic neurites that displayed a swollen/globular appearance positive for Gallyas silver staining was preferentially located in the subiculum (Fig. 2E1) and the stratum oriens of CA1 hippocampal subfield (Fig. 2E3) in the 3xTg-AD compared to 3xTg-AD/mtauKO mice (Fig. 2E2 and E4). Therefore, these results suggest that the endogenous tau appears to co-aggregate with human tau and contributes to the formation of NFTs in the 3xTg-AD mice.

3xTgAD/mtauKO mice express lower levels of tau hyper-phosphorylated at residues Thr-181 and Ser396/404 compared to 3xTg-AD mice

We next examined phosphorylation states of tau in soluble homogenate samples. Western blot analyses revealed a significant decrease in tau phosphorylated at residues Thr181 (86.27 ± 3.06%, ***p < 0.001, *t*-test recognized by the AT270 antibody) and Ser396/404 (73.15 ± 8.21%, ***p < 0.001, *t*-test recognized by the PHF-1 antibody) in the 3xTg-AD/mtauKO compared to 3xTg-AD mice. Levels of phospho-tau species recognized by antibodies AT8 (Ser199/202), AT100 (Ser214) and AT180 (Thr231) were unaltered in the 3xTg-AD/mtauKO compared to 3xTg-AD mice (Figs. 3A–B), this might imply a relative increase of tau phosphorylated in 3xTg-AD/mtauKO mice at these epitopes or no phosphorylation of endogenous tau at baseline. No differences in total human tau were seen between the 3xTg-AD and 3xTg-AD/mtauKO mice, suggesting that the presence of the endogenous murine tau did not alter the expression of human tau transgene (Figs. 3A and B). Moreover, western blot analysis of Ntg mice shows very low levels of tau phosphorylated at residues Thr181 and Ser396/404 compared to 3xTg-AD (Supplemental Figs. 1A and B). Therefore, these data suggest that endogenous tau, that is lowly phosphorylated at baseline level, is being hyperphosphorylated at these specific epitopes (Thr181 and Ser396/404) and promotes the formation of tau pathology in 3xTg-AD mice.

Furthermore, we observed a greater number of hippocampal pyramidal-cells with somatic accumulation of tau hyperphosphorylated at Ser396/404 (using PHF1 antibody) in 3xTg-AD compared to 3xTg-AD/mtauKO mice (31.01 ± 8.01%, *p < 0.05, *t*-test) (Figs. 3C–D). Interestingly, 3xTg-AD/mtauKO showed a significant accumulation of tau hyperphosphorylated at Ser 396/404 in both somatic and dendritic (arrow) compartments (Supplemental Fig. 2). However, 3xTg-AD mice mainly accumulate tau hyperphosphorylated at Ser 396/404 in the somatic compartment (Supplemental Fig. 2). Overall, these results indicate that murine tau is hyperphosphorylated in 3xTg-AD mice and contributing to the formation of NFTs.

3xTg-AD and 3xTg-AD/mtauKO mice express similar high levels of the cytosolic activator of cdk5, p25 compared to Ntg and mtauKO mice

We examined the total and activated forms of the two major kinases involved in tau phosphorylation, cyclin-dependent Kinase 5 (cdk5) and Glycogen synthase kinase 3-beta (GSK3β) (Medeiros et al., 2011) in Ntg, mtauKO, 3xTg-AD and 3xTg-AD/mtauKO mice. Western blot analyses revealed a significant increase in the cytosolic activator of cdk5, p25 in 3xTg-AD mice compared to Ntg (223.30 ± 32.33% one way ANOVA, Bonferroni post-hoc **p < 0.01) and mtauKO (313.58 ± 45.40% one way ANOVA, Bonferroni post-hoc **p < 0.01) mice. Furthermore, similar data were observed in 3xTg-AD/mtauKO mice compared to Ntg (204.62 ± 45.47% one way ANOVA, Bonferroni post-hoc **p < 0.01) and mtauKO (244.49 ± 42.82% one way ANOVA, Bonferroni post-hoc **p < 0.01) mice. No changes in steady-state levels of cdk5 and the cytosolic activators of cdk5, p35 were seen (Figs. 3E–F). Similarly, no differences in the inactivate and active GSK3β, detected by the phosphorylation at Ser9 and Tyr 216 residues respectively, were seen (Figs. 3E–F) (Grimes and Jope, 2001). Overall, the results indicate that aged 3xTg-AD and 3xTg-AD/mice show a significant activation of cdk5 compared to Ntg and mtauKO mice thus promoting the formation and accumulation of hyperphosphorylated tau forms. Notably, no differences were observed between 3xTg-AD compared to 3xTg-AD/mtauKO mice in both cdk5 and GSK3β.

Endogenous tau deletion in the 3xTg-AD mice does not alter Aβ pathology

We further examined whether the deletion of the endogenous murine tau in the 3xTg-AD led to any change in APP processing and/or Aβ deposition. Steady-state levels of full-length APP holoprotein were unaffected

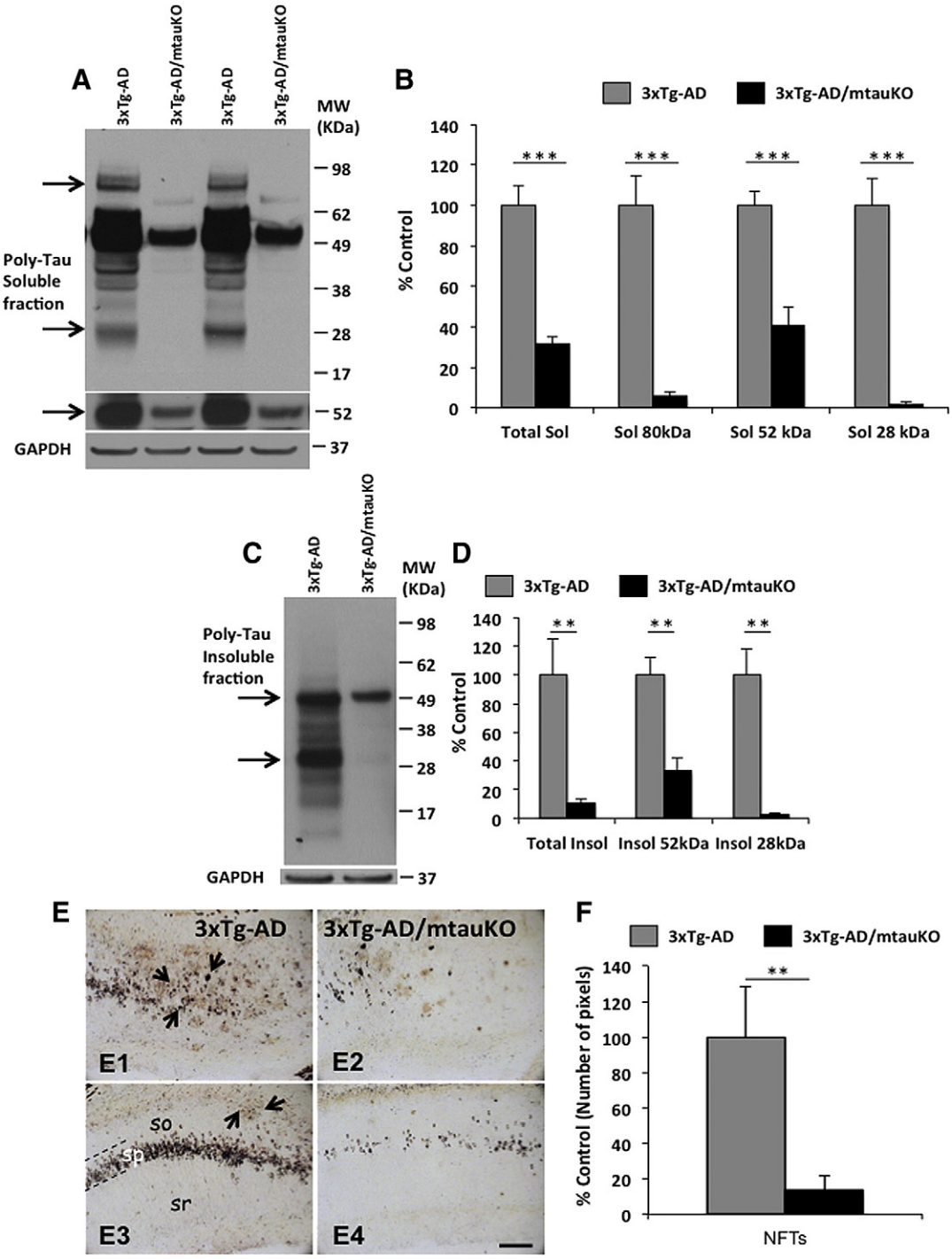

Fig. 2. Higher soluble and insoluble tau levels in 3xTg-AD compared to 3xTg-AD/mtauKO mice. A) Immunoblot analysis of tau (poly-tau) expression from soluble whole-brain homogenates in 3xTg-AD and 3xTg-AD/mtauKO mice at 18 month-old (n = 8) shown as alternating lanes. B) Quantification of A normalized to GAPDH and expressed as a % of control shows significant decreases on total soluble tau levels (68.50 ± 3.81%, ***p < 0.001, *t*-test) and tau fragments at 80 kDa (94.40 ± 2.49%, ***p < 0.001, *t*-test) and 28 kDa (97.11 ± 0.49%, **p < 0.01, *t*-test) in 3xTg-AD compared to 3xTg-AD/mtauKO mice (arrow). C) Immunoblot analysis of tau expression from insoluble whole-brain homogenates in 3xTg-AD and 3xTg-AD/mtauKO mice at 18 month-old (n = 8) shown as alternating lanes. D) Quantification of C normalized to GAPDH and expressed as a % of control shows significant decreases on total insoluble tau levels (89.32 ± 2.40%, **p < 0.01, *t*-test) and insoluble tau fragments at 52 kDa (66.93 ± 9.35%, **p < 0.01, *t*-test) and 28 kDa (97.11 ± 0.49%, **p < 0.01, *t*-test) in 3xTg-AD compared to 3xTg-AD/mtauKO mice (arrow). E) Representative hippocampal sections, subiculum (E1 and E2) and CA1 (E3 and E4) subfield in 3xTg-AD (E1 and E3) and 3xTg-AD/mtauKO (E2 and E4) at 18 month-old mice, showing significant intraneuronal NFT accumulations, as detected by Gallyas silver staining (86.33 ± 28.17%, **p < 0.01, *t*-test). The presence of dystrophic neurites (arrows) was observed in the subiculum (E1) and stratum oriens (E3) of 3xTg-AD mice. so: stratum oriens; sp: stratum pyramidale; slm: stratum lacunosum-moleculare. Scale bars: 100 μm (E1 and E4). The values represent the mean ± S.E.M. **p < 0.01 and ***p < 0.001.

by western-blot analysis between 3xTg-AD and 3xTg-AD/mtauKO mice (Figs. 4A and B). Similarly, the C-terminal fragments (CTFs) C83 and C99, which are membrane stubs produced by cleavage of APP by α-secretase and BACE1, respectively, were not altered between 3xTg-AD and 3xTg-AD/mtauKO (Figs. 4A and B). The soluble and insoluble Aβ levels, measured by sandwich ELISA, were also unchanged between the 3xTg-AD and 3xTg-AD/mtauKO mice (Figs. 4C and D). Consistent with the ELISA results, immunohistological analysis with the antibody 6E10

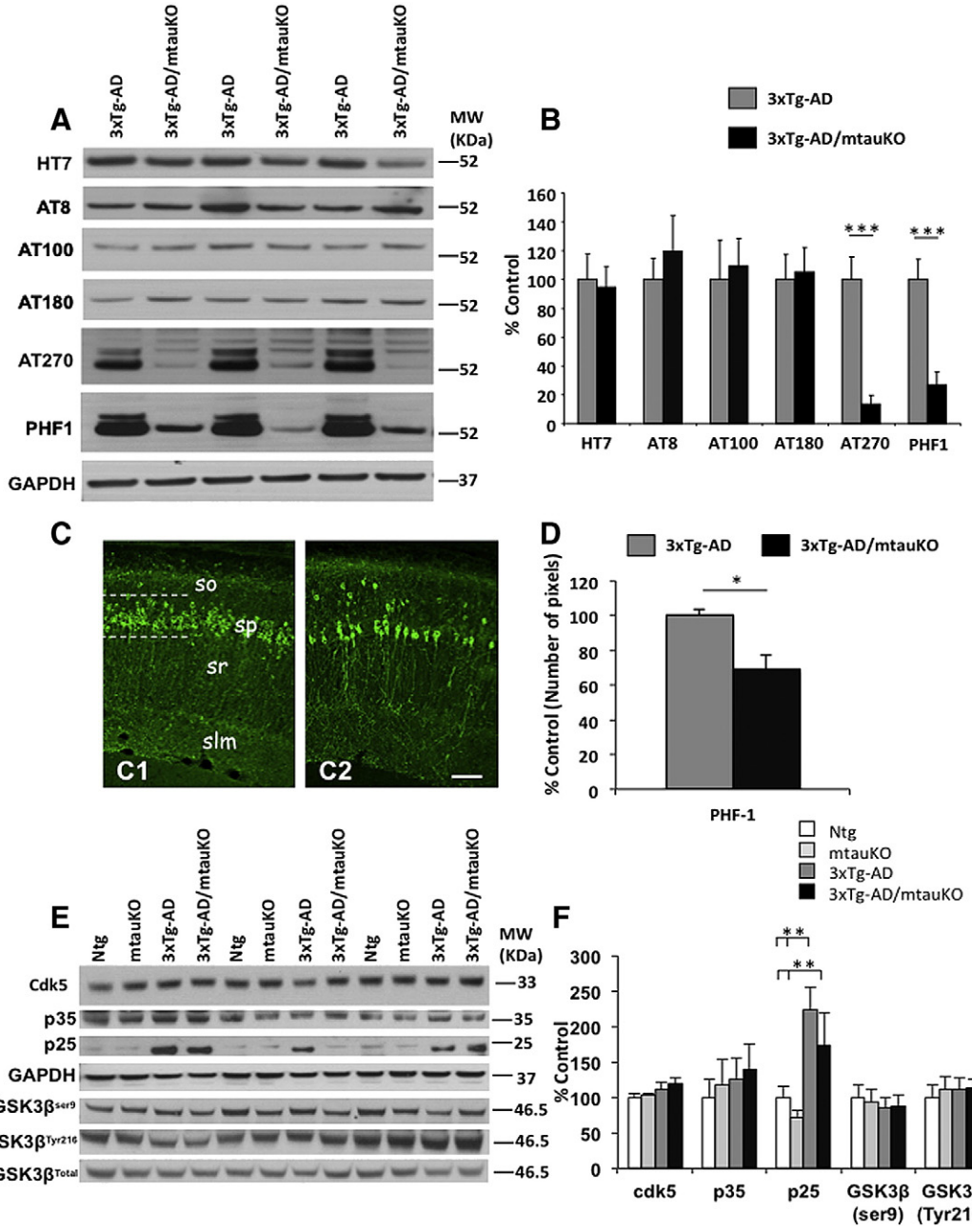

Fig. 3. 3xTg-AD mice show significant increases in soluble-tau hyperphosphorylated at Thr181 and Ser396/404 compared to 3xTg-AD/mtauKO mice. A) Immunoblot analysis of total human tau (HT7) and phospho-tau epitopes including pSer199/202 (AT8), pThr212/Ser 214 (AT100), pThr231 (AT180), pThr181 (AT270) and pSer396/404 (PHF-1) of protein extracts from whole-brain homogenates of 3xTg-AD and 3xTg-AD/mtauKO mice at 18 month-old (n = 8) shown as alternating lanes. B) Quantification of A normalized to GAPDH and expressed as a % of control shows significant decreases in p-tau epitopes at 18 month-old at Thr181 (86.27 ± 3.06%, ***p < 0.001, *t*-test) and Ser 396/404 (73.15 ± 8.21%, ***p < 0.001, *t*-test) in the 3xTg-AD/mtauKO compared to 3xTg-AD mice. C) Representative immunofluorescent confocal laser scanning image using PHF-1 antibody in hippocampal sections (CA1 subfield) in 3xTg-AD (C1) and 3xTg-AD/mtauKO (C2) mice at 18 month-old, showing mainly somatic phospho-tau accumulation in the 3xTg-AD and a somatodendritic phospho-tau accumulation in the 3xTg-AD/mtauKO. D) Quantification of PHF-1 expression in CA1 hippocampal subfield shows a significant decrease of PHF-1 immunoreactivity in 3xTg-AD/mtauKO compared to 3xTg-AD mice (31.01 ± 8.01%, *p < 0.05, *t*-test). E) Immunoblot analysis of cdk5, p25/p35 and inactive GSK3β (phosphorylated at ser9 and tyr216) of protein extracts from whole-brain homogenates of 3xTg-AD and 3xTg-AD/mtauKO mice (n = 8) at 18 month-old shown as alternating lanes. F) Quantification of E normalized to GAPDH and total GSK3β and expressed as a % of control shows significant increases in the expression of p25 in 3xTg-AD compared to Ntg (223.30 ± 32.33% one way ANOVA, Bonferroni post-hoc **p < 0.01) and mtauKO (313.58 ± 45.40% one way ANOVA, Bonferroni post-hoc **p < 0.01) mice. In addition, 3xTg-AD/mtauKO mice show significant increases in the expression of p25 compared to Ntg (204.62 ± 45.47% one way ANOVA, Bonferroni post-hoc **p < 0.01) and mtauKO (244.49 ± 42.82% one way ANOVA, Bonferroni post-hoc **p < 0.01) mice. Furthermore, no differences were observed in cdk5, p35 and GSK3β (ser9 and tyr216) expression in all genotype analyzed (Ntg, mtauKO, 3xTg-AD and 3xTg-AD/mtauKO). GAPDH and GSK3β levels were used as control for protein loading. Scale bars: 200 μm (C1 and C2). The values represent the mean ± S.E.M. *p < 0.05, **p < 0.01 and ***p < 0.001.

showed no difference in the intra/extra-cellular immunolabeling expression pattern of APP/Aβ in the 3xTg-AD and 3xTg-AD/mtauKO mice (Fig. 4E). These results are consistent with previous studies showing that tau reduction (Roberson et al., 2007) or a genetic modulation of tau (Oddo et al., 2007) does not influence Aβ pathology.

Endogenous mouse tau deletion does not alter hippocampal-dependent cognition in 3xTg-AD mice

Previous studies showed that crossing tau knockout mice with human APP rescued cognitive deficits and axonal transporter in hAPP

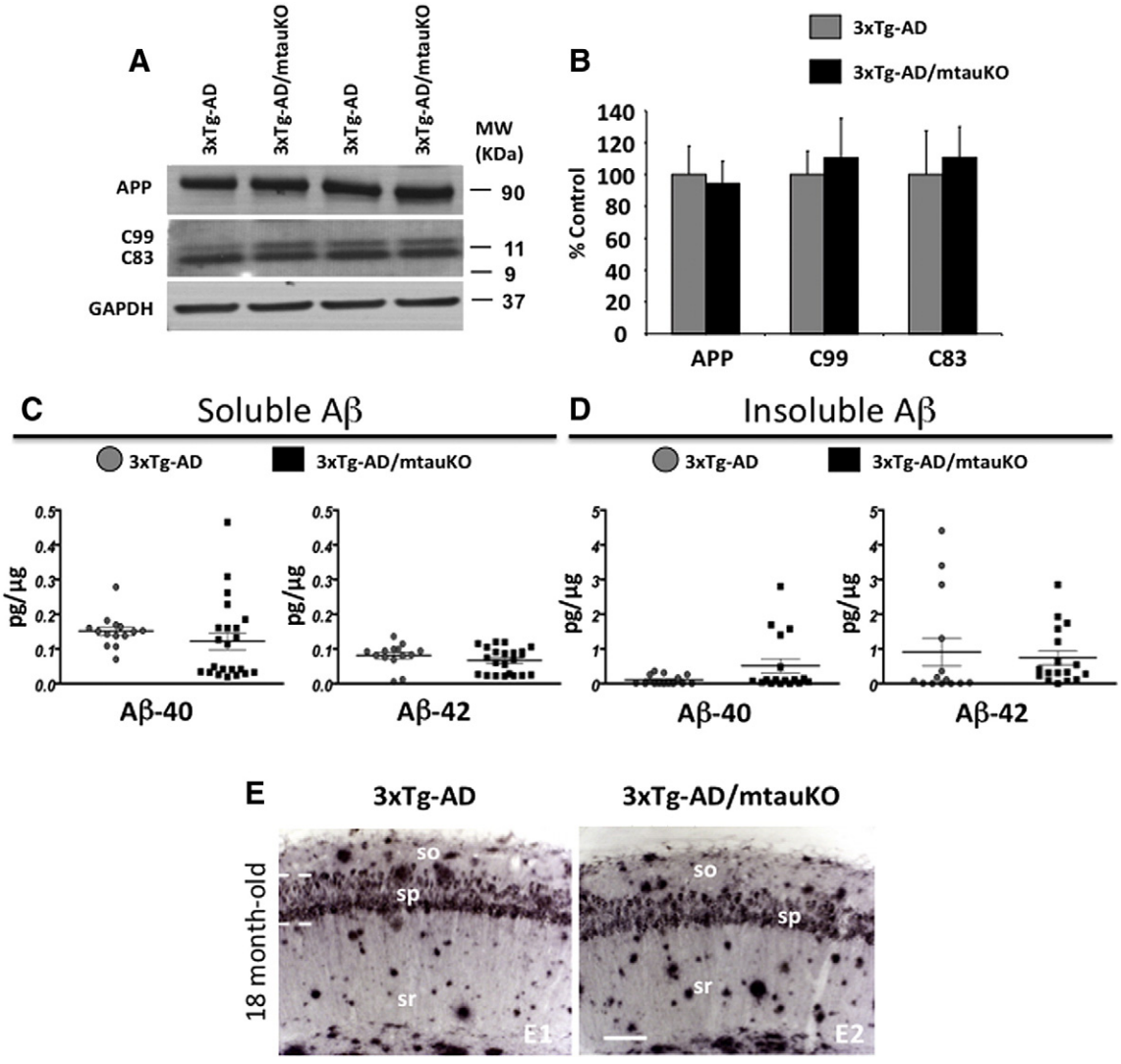

Fig. 4. Deletion of mouse tau in the 3xTg-AD did not change Aβ pathology. A) Immunoblot analysis of APP holoprotein, C99 and C83 C-terminal APP fragment from whole-brain homogenates of 3xTg-AD and 3xTg-AD/mtauKO mice at 18 month-old shown as alternating lanes. B) Quantification of A normalized to GAPDH and expressed, as a % of control shows no differences in 3xTgAD compared to 3xTgAD/mtauKO mice. C–D) Brain Aβ measurements by sandwich ELISA of both the soluble (C) and insoluble (D), Aβ40 and Aβ42 fractions of 3xTg-AD and 3xTg-AD/mtauKO mice at 18 month-old revealed no significant differences in Aβ levels. E) Light microscopic images immunostained with anti-Aβ antibody (6E10) in the hippocampus (CA1 areas) of 3xTg-AD (E1) and 3xTg-AD/mtauKO (E2) 18 month-old. so: stratum oriens; sp: stratum pyramidale; sr: stratum radiatum. Scale bars: 100 µm (E1–E2).

mice (hAPPJ20) (Medeiros et al., 2011; Roberson et al., 2007). However, when human tau is present and endogenous tau is knocked out, a significant increase and acceleration of pathological tau assemblies are seen in mice (Ando et al., 2011; Andorfer et al., 2003). Therefore, to address the impact of endogenous mouse tau on cognition, Ntg, mtauKO, 3xTg-AD and 3xTgAD/mtauKO mice were tested on a battery of behavioral tasks.

Mice were first tested on novel context and place tasks. These tasks are mainly hippocampal dependent. Both, 3xTg-AD and 3xTg-AD/mtauKO mice were significantly impaired compared to Ntg mice on the novel context and place, spending 51.56 ± 3.92% (3xTg-AD) and 51.02 ± 2.25% (3xTg-AD/mtauKO) of their time exploring the out-of-context object, 49.44 ± 3.75% (3xTg-AD) and 50.49 ± 1.80% (3xTg-AD/mtauKO) of their time exploring the out-of-place object (Figs. 5A and B), compared to Ntg mice. Notably, no differences were observed between 3xTg-AD and 3xTg-AD/mtauKO mice (Figs. 5A and B).

Next, mice were trained to criterion (escape latency <25 s) in the spatial reference version of MWM to find the location of a hidden platform. Significant differences were found in Ntg compared to 3xTg-AD and 3xTg-AD/mtauKO mice. Ntg mice reached criterion in 5 days, mtauKO mice required 7 days, and both 3xTg-AD and 3xTg-AD/mtauKO mice did not reach criterion after 7 days of training. Furthermore, no differences were observed on acquisition memory in 3xTg-AD compared to 3xTg-AD/mtauKO mice and Ntg compared to mtauKO mice at this age (Fig. 5C).

Retention memory was tested 24 h after the last training trial. We found that 3xTg-AD (30.19 ± 7.93% one way ANOVA, Bonferroni post-hoc $^{**}p < 0.01$) and 3xTg-AD/mtauKO (25.83 ± 8.02% one way ANOVA, Bonferroni post-hoc $^{**}p < 0.01$) mice show significant decreases on time spent in the platform quadrant compared to Ntg. Notably, no differences were observed between 3xTg-AD and 3xTg-AD/mtauKO mice (Fig. 5D). Additionally, we found significant increases in the time spent in the opposite zone in 3xTg-AD (176.98 ± 60.17% one way ANOVA, Bonferroni post-hoc $^{***}p < 0.001$) and 3xTg-AD/mtauKO (154.73 ± 26.69% one way ANOVA, Bonferroni post-hoc $^{*}p < 0.05$) compared to Ntg mice. Similar increases in the time spent in the opposite zone were obtained in 3xTg-AD (150.20 ± 46.45% one way ANOVA, Bonferroni post-hoc $^{***}p < 0.001$) and 3xTg-AD/mtauKO (130.19 ± 24.13% one way ANOVA, Bonferroni post-hoc $^{*}p < 0.05$) compared to mtauKO mice (Fig. 5E). The observed differences in cognition were not due to motor impairments, as swim speed or total travel distance was similar among the groups (data not shown).

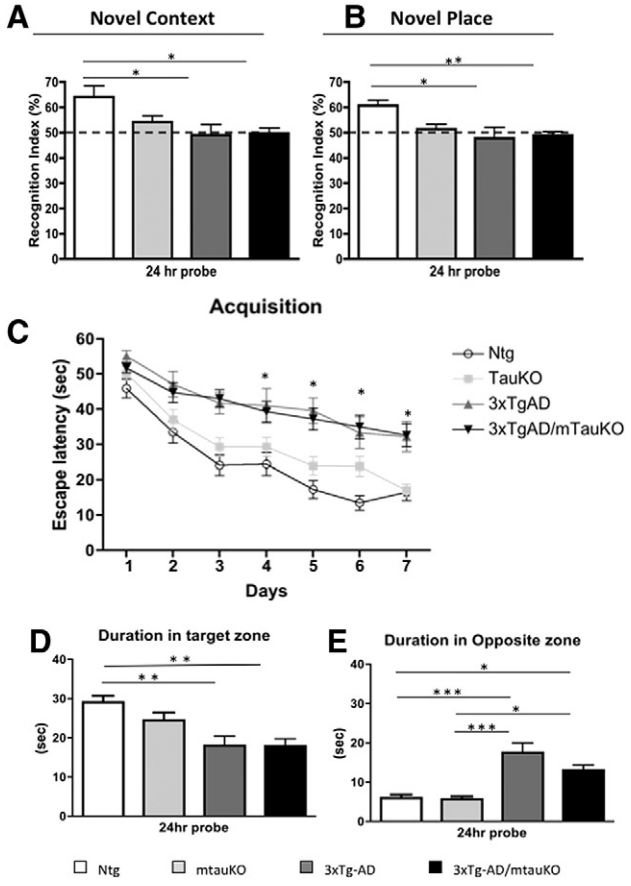

Fig. 5. Depletion of mouse tau in the 3xTg-AD mice did not alter hippocampal cognitive impairment. A and B) Significant impairment in memory by novel context (A) and place (B) recognition was observed in both 3xTg-AD and 3xTg-AD/mtauKO compared to Ntg mice. D–E) Mice were trained on the spatial reference version of the Morris water maze (MWM; n = 16–20 per group) at 18 (D–E) month-old. (D) Acquisition curves shown for the 7 days of training on MWM show significant differences in Ntg and mtauKO mice compared to 3xTg-AD and 3xTg-AD mice. Notably, no differences were observed in 3xTg-AD versus 3xTg-AD/mtauKO mice. D) Significant differences were observed in Ntg versus 3xTg-AD mice (30.19 ± 7.93% one way ANOVA, Bonferroni post-hoc $^{**}p < 0.01$) and in Ntg versus 3xTg-AD/mtauKO mice (25.83 ± 8.02% one way ANOVA, Bonferroni post-hoc $^{**}p < 0.01$) in the time spent in the target zone. E) Significant increase on time spending in the opposite zone was observed in 3xTg-AD versus Ntg mice (150.20 ± 46.45% one way ANOVA, Bonferroni post-hoc $^{***}p < 0.001$) and 3xTg-AD/mtauKO versus Ntg (130.19 ± 24.13% one way ANOVA, Bonferroni post-hoc $^{*}p < 0.05$). The values represent the mean ± S.E.M. (N = 16–20). $^{*}p < 0.05$, $^{**}p < 0.01$ and $^{***}p < 0.001$.

Overall, the data suggest that endogenous tau promotes tau pathology in 3xTg-AD mice without affecting cognition. However, further studies in younger ages will be necessary to corroborate the current data, where the increase on tau pathology observed in 3xTg-AD did not further impair cognition as compared to 3xTg-AD/mtauKO mice.

Discussion

To better understand the role of endogenous murine tau in the pathological events that occur in AD models and its interaction with Aβ-peptide, we developed a novel transgenic mouse model referred to as 3xTg-AD/mtauKO. This mouse overexpresses APP695SWE and tauP301L under the control of the thy1.2 promoter, and the presenilin 1 M146V knockin mutation. Finally, it has its endogenous murine tau knocked out. Hence, 3xTg-AD mice have both endogenous and human tau, while 3xTg-AD/mtauKO mice express only human tau in neurons in the hippocampus, cortex and amygdala. Our results indicate that endogenous murine tau contributes to the progression of tau pathology in the 3xTg-AD mice with considerable increases in NFT formation. As 3xTg-AD mice have much higher levels of phosphorylated tau and insoluble tau than 3xTg-AD/mtauKO mice, it suggests that the endogenous murine tau is being incorporated into the tau pathology. In addition, we showed that Ntg mice have low levels of phosphorylated tau at baseline. Hence, these data suggest that endogenous tau, that is poorly phosphorylated at baseline level, is being hyperphosphorylated in 3xTg-AD mice and incorporating into the tau pathology.

A previous study showed that Aβ is able to induce hyperphosphorylation of endogenous tau in Tg2576 mice (Otth et al., 2002), which is necessary for cognitive impairments. Additionally, we showed in 3xTg-AD mice that Aβ is involved in the onset and progression of tau pathology via the C-terminus of heat shock protein 70-interacting protein (CHIP) (Oddo et al., 2008). Therefore, Aβ in 3xTg-AD mice must trigger hyperphosphorylation of endogenous murine tau at specific epitopes (Thr-181 and Ser396/404), and it likely becomes incorporated into NFTs and detergent-insoluble tau accumulations. These findings contradict several studies that show murine tau has anti-aggregation properties due to sequences with its N-terminus (Ando et al., 2010), and that crossing tau knockout mice with human tau models accelerates tau assembly (Ando et al., 2011; Andorfer et al., 2003). However, in agreement with our data, other studies show that endogenous murine tau is capable of assembling PHFs and co-aggregating with human truncated tau (Chohan et al., 2005; Kampers et al., 1999; Mocanu et al., 2008; Sydow and Mandelkow). Although, we used a different mtauKO strain compared to previous studies (Ando et al., 2011; Andorfer et al., 2003), we consider that the differences observed in our current study might be related to the presence of both Aβ and tau in our model compared rather than human tau alone (Ando et al., 2011; Andorfer et al., 2003).

This study shows that 3xTg-AD mice have an increase in the level of tau hyperphosphorylated and NFT aggregates compared to 3xTg-AD/mtauKO mice. However, despite these increases in tau pathology, it does not have an influence on cognitive function in the 3xTg-AD mice. Accordingly, recent studies suggest that NFTs may not be pathogenic but rather could be a neuroprotective response to other disease stimuli, such as oxidative stress or inflammation (Andorfer et al., 2005; Santacruz et al., 2005; Wittmann et al., 2001). Specifically, it has been shown in an inducible tau model that, after repression of tau expression, tau hyperphosphorylation and tangle formation progressed while memory function was recovered (Santacruz et al., 2005). In addition, it has been shown that NFT toxicity is not the only cause of the dramatic neuronal loss observed in mice expressing normal human tau (Andorfer et al., 2005). Therefore, these increases in NFT aggregates observed in 3xTg-AD mice may not be directly related with an impairment of cognitive deficit.

Hence, our study suggests that endogenous murine tau contributes to the progression of AD pathology in the presence of human Aβ and tau. However, this increase in tau pathology does not cause any further detectable deterioration in learning and memory. We believe that 3xTg-AD/mtauKO mice represent a better AD model to understand the molecular interaction between human Aβ and tau, as the confounding variable of non-human endogenous tau has been removed. Overall, our study provides relevant insights to better understand the contribution of endogenous tau to AD pathology and for developing new AD models.

Supplementary data to this article can be found online at http://dx.doi.org/10.1016/j.nbd.2013.10.019.

Author contributions

D.B.V, M.K, K.N.G and F.M.L., designed the experiments. D.B.V., E.J.L., T.E.H., performed experiments. C.J.R.O. performed the statistical analyses. D.B.V., M.K., C.J.R.O., R. M., K.N.G., and F.M.L., wrote the manuscript, and F.M.L. contributed financially to the studies.

Conflict of interest

No potential conflicts of interest relevant to this article were reported.

Acknowledgments

We would like to thank Dr. Agenor Limon and Dr. Rahasson Ager for comments on a previous version of the manuscript. This study was supported by grant from the National Institute of Health (NIH): NIH/NIA AG027544 and AG021982 (F.M.L.). Aβ peptides and anti-Aβ antibodies were provided by the University of California Alzheimer's Disease Research Center (UCI-ADRC) NIH/NIA Grant P50 AG16573.

References

Ando, K., et al., 2010. Deletion of murine tau gene increases tau aggregation in a human mutant tau transgenic mouse model. Biochem. Soc. Trans. 38, 1001–1005.
Ando, K., et al., 2011. Accelerated human mutant tau aggregation by knocking out murine tau in a transgenic mouse model. Am. J. Pathol. 178, 803–816.
Andorfer, C., et al., 2003. Hyperphosphorylation and aggregation of tau in mice expressing normal human tau isoforms. J. Neurochem. 86, 582–590.
Andorfer, C., et al., 2005. Cell-cycle reentry and cell death in transgenic mice expressing nonmutant human tau isoforms. J. Neurosci. 25, 5446–5454.
Baglietto-Vargas, D., et al., 2013. Mifepristone alters amyloid precursor protein processing to preclude amyloid beta and also reduces tau pathology. Biol. Psychiatry 74 (5), 357–366.
Billings, L.M., et al., 2005. Intraneuronal Abeta causes the onset of early Alzheimer's disease-related cognitive deficits in transgenic mice. Neuron 45, 675–688.
Braak, H., et al., 1988. Silver impregnation of Alzheimer's neurofibrillary changes counterstained for basophilic material and lipofuscin pigment. Stain. Technol. 63, 197–200.
Brion, J.P., et al., 1999. Transgenic expression of the shortest human tau affects its compartmentalization and its phosphorylation as in the pretangle stage of Alzheimer's disease. Am. J. Pathol. 154, 255–270.
Chohan, M.O., et al., 2005. Hyperphosphorylation-induced self assembly of murine tau: a comparison with human tau. J. Neural Transm. 112, 1035–1047.
Dawson, H.N., et al., 2001. Inhibition of neuronal maturation in primary hippocampal neurons from tau deficient mice. J. Cell Sci. 114, 1179–1187.
Denk, F., Wade-Martins, R., 2009. Knock-out and transgenic mouse models of tauopathies. Neurobiol. Aging 30, 1–13.
Duff, K., et al., 2000. Characterization of pathology in transgenic mice over-expressing human genomic and cDNA tau transgenes. Neurobiol. Dis. 7, 87–98.
Fic, E., et al., 2010. Comparison of protein precipitation methods for various rat brain structures prior to proteomic analysis. Electrophoresis 31, 3573–3579.
Gallyas, F., 1971. Silver staining of Alzheimer's neurofibrillary changes by means of physical development. Acta Morphol. Acad. Sci. Hung. 19, 1–8.
Gotz, J., et al., 1995. Somatodendritic localization and hyperphosphorylation of tau protein in transgenic mice expressing the longest human brain tau isoform. EMBO J. 14, 1304–1313.
Gotz, J., et al., 2001. Formation of neurofibrillary tangles in P301l tau transgenic mice induced by Abeta 42 fibrils. Science 293, 1491–1495.
Grimes, C.A., Jope, R.S., 2001. The multifaceted roles of glycogen synthase kinase 3beta in cellular signaling. Prog. Neurobiol. 65, 391–426.
Hernandez, F., Avila, J., 2007. Tauopathies. Cell. Mol. Life Sci. 64, 2219–2233.
Higuchi, M., et al., 2002. Transgenic mouse model of tauopathies with glial pathology and nervous system degeneration. Neuron 35, 433–446.
Ishihara, T., et al., 1999. Age-dependent emergence and progression of a tauopathy in transgenic mice overexpressing the shortest human tau isoform. Neuron 24, 751–762.
Ishihara, T., et al., 2001. Age-dependent induction of congophilic neurofibrillary tau inclusions in tau transgenic mice. Am. J. Pathol. 158, 555–562.
Kampers, T., et al., 1999. Assembly of paired helical filaments from mouse tau: implications for the neurofibrillary pathology in transgenic mouse models for Alzheimer's disease. FEBS Lett. 451, 39–44.
Lewis, J., et al., 2001. Enhanced neurofibrillary degeneration in transgenic mice expressing mutant tau and APP. Science 293, 1487–1491.
Medeiros, R., et al., 2011. The role of tau in Alzheimer's disease and related disorders. CNS Neurosci. Ther. 17, 514–524.
Mocanu, M.M., et al., 2008. The potential for beta-structure in the repeat domain of tau protein determines aggregation, synaptic decay, neuronal loss, and coassembly with endogenous Tau in inducible mouse models of tauopathy. J. Neurosci. 28, 737–748.
Oddo, S., et al., 2003. Triple-transgenic model of Alzheimer's disease with plaques and tangles: intracellular Abeta and synaptic dysfunction. Neuron 39, 409–421.
Oddo, S., et al., 2004. Abeta immunotherapy leads to clearance of early, but not late, hyperphosphorylated tau aggregates via the proteasome. Neuron 43, 321–332.
Oddo, S., et al., 2007. Genetically augmenting tau levels does not modulate the onset or progression of Abeta pathology in transgenic mice. J. Neurochem. 102, 1053–1063.
Oddo, S., et al., 2008. Blocking Abeta42 accumulation delays the onset and progression of tau pathology via the C terminus of heat shock protein70-interacting protein: a mechanistic link between Abeta and tau pathology. J. Neurosci. 28, 12163–12175.
Otth, C., et al., 2002. AbetaPP induces cdk5-dependent tau hyperphosphorylation in transgenic mice Tg2576. J. Alzheimers Dis. 4, 417–430.
Probst, A., et al., 2000. Axonopathy and amyotrophy in mice transgenic for human four-repeat tau protein. Acta Neuropathol. 99, 469–481.
Querfurth, H.W., LaFerla, F.M., 2010. Alzheimer's disease. N. Engl. J. Med. 362, 329–344.
Roberson, E.D., et al., 2007. Reducing endogenous tau ameliorates amyloid beta-induced deficits in an Alzheimer's disease mouse model. Science 316, 750–754.
Santacruz, K., et al., 2005. Tau suppression in a neurodegenerative mouse model improves memory function. Science 309, 476–481.
Shipton, O.A., et al., 2011. Tau protein is required for amyloid {beta}-induced impairment of hippocampal long-term potentiation. J. Neurosci. 31, 1688–1692.
Sydow, A., Mandelkow, E. M., 'Prion-like' propagation of mouse and human tau aggregates in an inducible mouse model of tauopathy. Neurodegener Dis. 7, 28–31.
Terwel, D., et al., 2002. Axonal transport, tau protein, and neurodegeneration in Alzheimer's disease. Neuromol. Med. 2, 151–165.
Tseng, B.P., et al., 2008. Abeta inhibits the proteasome and enhances amyloid and tau accumulation. Neurobiol. Aging 29, 1607–1618.
Wittmann, C.W., et al., 2001. Tauopathy in Drosophila: neurodegeneration without neurofibrillary tangles. Science 293, 711–714.